Understanding the dynamics of photoionization-induced nonlinear effects and solitons in gas-filled hollow-core photonic crystal fibers

Mohammed F. Saleh* and Fabio Biancalana
Max Planck Institute for the Science of Light, Günther-Scharowsky Str. 1, DE-91058 Erlangen, Germany
(Received 20 October 2011; published 16 December 2011)

We present the details of our previously formulated model [Saleh *et al.*, Phys. Rev. Lett. **107**, 203902 (2011)] that governs pulse propagation in hollow-core photonic crystal fibers filled by an ionizable gas. By using perturbative methods, we find that the photoionization process induces the opposite phenomenon of the well-known Raman self-frequency redshift of solitons in solid-core glass fibers, as was recently experimentally demonstrated [Hölzer *et al.*, Phys. Rev. Lett. **107**, 203901 (2011)]. This process is only limited by ionization losses, and leads to a constant acceleration of solitons in the time domain with a continuous blueshift in the frequency domain. By applying the Gagnon-Bélanger gauge transformation, multipeak "inverted gravitylike" solitary waves are predicted. We also demonstrate that the pulse dynamics shows the ejection of solitons during propagation in such fibers, analogous to what happens in conventional solid-core fibers. Moreover, unconventional long-range nonlocal interactions between temporally distant solitons, unique of gas plasma systems, are predicted and studied. Finally, the effects of higher-order dispersion coefficients and the shock operator on the pulse dynamics are investigated, showing that the conversion efficiency of resonant radiation into the deep UV can be improved via plasma formation.

DOI: 10.1103/PhysRevA.84.063838 PACS number(s): 42.65.Tg, 42.81.Dp, 52.35.Sb

I. INTRODUCTION

The invention of photonic crystal fibers (PCFs) has led to a revolution in the field of nonlinear fiber optics [1]. Hollow-core PCFs (HC-PCFs) with the so-called kagomé-lattice claddings have recently become a superior host for the investigation of light-matter interactions between intense ultrashort optical pulses and gaseous or liquid media [2]. These fibers are characterized by a broadband transmission range with low group-velocity dispersion (GVD) and a high confinement of light in the core [3]. Many important phenomena have already been observed in HC-PCFs. For instance, a drastic reduction in the Raman threshold has been shown in H_2-filled HC-PCFs [4]. These fibers have also been used to generate solitary pulses by backward stimulated Raman scattering [5] and to observe self-similarity in the evolution of transient stimulated Raman scattering [6]. Important applications such as high-harmonic [7] and efficient deep UV generation [8] have been recently demonstrated in HC-PCFs filled with noble gases, which do not suffer the limitations introduced by the Raman effect.

Intrapulse Raman scattering allows for a continuous down-conversion of the central wavelength of a pulse propagating in an optical fiber, due to the continuous conversion of energy of the coherent pulse into incoherent optical phonons always present in the medium. Dianov *et al.* have made the first observation of an efficient energy redshift from a pulse maximum to its tail via the Raman effect [9]. This has been followed by an experimental demonstration of the soliton self-frequency redshift in optical fibers [10], theoretically described in Refs. [11,12]. Thereafter, the Raman process has been extensively studied and exploited in the field of nonlinear fiber optics [13–16]—a notable example is supercontinuum generation in PCFs [17].

Historically, the concept of soliton blueshift has been originally introduced and predicted in Ref. [18]. In tapered solid-core photonic crystal fibers, soliton blueshift has been observed due to the variation of the zero-dispersion wavelength (ZDW) along the fiber [19]. In the photoionization regime, a limited (of only a few nanometers) ionization-induced blueshift of guided ultrashort pulses has been predicted in conventional gas-filled photonic band-gap HC-PCFs, which suffer large group-velocity dispersion variations near the band edges, thus preventing the clear formation of solitary waves [20,21]. Very recently, however, a sequence of emitted strong blueshifted pulses has been observed in a groundbreaking experiment involving Ar-filled kagomé-style HC-PCFs, by using few-μJ fs laser pulses [22,23]. The use of the kagomé HC-PCF in these experiments was essential due to its unique guiding features. Such fibers possess an unusual broadband guidance, and a remarkably small group-velocity dispersion (GVD) ($|\beta_2| < 10\ \mathrm{fs}^2/\mathrm{cm} \equiv 1\ \mathrm{ps}^2/\mathrm{km}$ from 400 nm to 1 μm) in comparison to the traditional solid-core fibers [8,23,24]. Moreover, the gas and waveguide contributions to the GVD can be balanced in the optical wavelength regime [24], unlike large-bore capillary-based systems, where the normal dispersion of the gas always dominates over the anomalous dispersion of the waveguide.

Prior to our present work on the optical nonlinearities induced by photoionization, Geissler *et al.* modeled the photoionization process in terms of the full electric field of the pulse [25], which is computationally very expensive. Recently, we have presented a model based on the evolution of the complex pulse envelope [26], which allows several interesting predictions, and it is more suitable for analytical and numerical investigation than other previously proposed models. The validity of the model has been carefully verified by using a numerical model [27] based on the unidirectional wave equation [28]. Our model allows us to use well-known analytical and numerical methods, developed to study pulse

*mohammed.saleh@mpl.mpg.de

 ©2011 American Physical Society

propagation in optical fibers, such as perturbation theory, the split-step Fourier method [16], and soliton particlelike analogy [29,30]. By using our model, (i) we derive analytical expressions for the soliton self-frequency blueshift in the presence and absence of the photoionization threshold of the gas, incidentally introducing the concept of floating solitons; (ii) we predict the possibility of observing two-peak "inverted gravitylike" solitons; and (iii) we explore the effects of higher-order dispersion and shock terms, demonstrating that a plasma-assisted blueshift can enhance the efficiency of resonant radiation in the UV, possibly improving previous experimental results [8]. Our theoretical results closely follow the experimental measurements in Ref. [23].

The paper is organized as follows. In Sec. II, the governing equations of pulse propagation in HC-PCFs filled with an ionizable gas are reviewed. In Sec. III, the perturbation theory is applied to study the effect of photoionization on the soliton amplitude, the temporal location of the soliton peak, and the self-frequency shift. The possibility of observing two-peak inverted gravitylike solitons is discussed in Sec. IV. Section V is dedicated to studying soliton dynamics in plasma. The effects of higher-order dispersion and shock terms on pulse propagation are examined in Sec. VI. Our conclusions are provided in Sec. VII.

II. GOVERNING EQUATIONS

Photoionization can take place by either tunneling or multiphoton processes. These regimes are characterized by the Keldysh parameter p_K [31,32]. For optical pulses with intensities in the range 100 TW/cm^2, the Keldysh parameter is in the limiting regime between the tunneling or multiphoton processes. In this case, the Yudin-Ivanov modification of the Perelomov-Popov-Terent'ev technique is considered to be the appropriate model since it accounts for both processes [33,34]. Experimental measurements [35,36] show that tunneling models [37,38] can well describe photoionization processes in noble gases for optical-pulse intensities in the range of TW/cm^2. This is also confirmed by recent calculations [27] based on the tunneling Ammosov-Delone-Krainov model [38] that reproduce simultaneous experimental results [23]. The time-averaged ionization rate $\mathcal{W}(I)$ can be expressed as [37–39]

$$\mathcal{W}(I) = c_1\, I^{-1/4}\, \exp(-c_2\, I^{-1/2}), \tag{1}$$

where c_1 and c_2 are constants and I is the laser-pulse intensity. As shown in Fig. 1(a), Eq. (1) predicts an ionization rate that has an exponential-like behavior for pulse intensities above a certain threshold value $I_{\rm th}$. Ionization-induced loss that is due to the absorption of photons during plasma formation is *proportional* to the ionization rate [32]. As a consequence, pulses with large intensities well above the threshold limit will have their intensities strongly driven back to near $I_{\rm th}$, where the ionization-induced loss is drastically reduced. This allows us to *linearize* Eq. (1) by using the first-order Taylor series in the proximity of $I_{\rm th}$, where pulses can survive without appreciable attenuation for a relatively long time. This is our concept of *floating pulses* introduced in Ref. [26] and shown in Fig. 1(b).

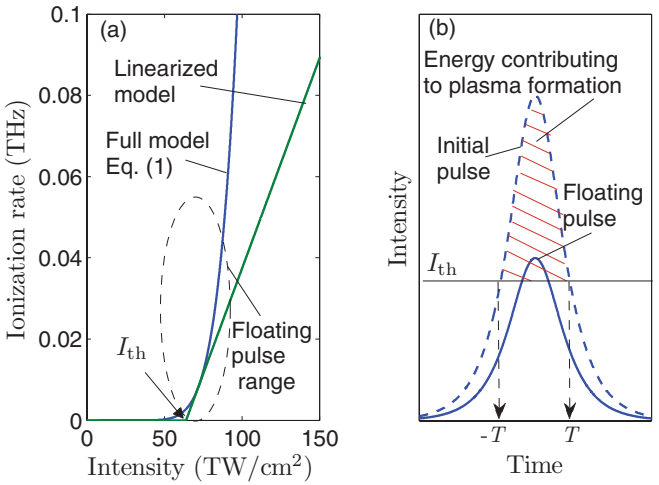

FIG. 1. (Color online) (a) Comparison of the dependence of the argon ionization rate on the pulse intensity using the full model of Eq. (1) and the linearized model of Eq. (2). (b) A sketch that represents the attenuation of an initial pulse to a floating pulse above the threshold limit due to ionization-induced loss.

Expanding Eq. (1) in its linear regime results in

$$\mathcal{W}(I) \approx \tilde{\sigma}\ (I - I_{\rm th})\ \Theta(I - I_{\rm th}), \tag{2}$$

where $I_{\rm th}$ and $\tilde{\sigma}$ can be related to c_1, c_2, and the expansion point, which is chosen to reproduce the physically observed threshold intensity of the considered gas [26]. The purpose of the Heaviside function Θ is to cut the ionization rate below $I_{\rm th}$. As shown in Fig. 1(a), the linearized model underestimates the ionization rate and the ionization losses, in comparison to the full model. This leads nevertheless to surprisingly similar qualitative behavior between the two models even for $I > I_{\rm th}$, since the strong ionization losses occurring well above the threshold tend to push the pulse amplitude toward the linearized region of the ionization rate.

By using Eq. (2), one can show that propagation of light in a HC-PCF filled with an ionized Raman-active gas can be modeled by the following coupled equations:

$$\left[i\partial_z + \hat{D}(i\partial_t) + \gamma_K R(t) \otimes |\Psi(t)|^2 - \frac{\omega_p^2}{2k_0 c^2} + i\tilde{\alpha} \right] \Psi = 0, \tag{3}$$

$$\partial_t n_e = [\tilde{\sigma}/A_{\rm eff}][n_T - n_e]\left[|\Psi|^2 - |\Psi|^2_{\rm th}\right]\Theta\left(|\Psi|^2 - |\Psi|^2_{\rm th}\right), \tag{4}$$

where $\Psi(z,t)$ is the electric-field *envelope*, z is the longitudinal coordinate along the fiber, t is the time coordinate in a reference frame moves with the pulse group velocity, $\hat{D}(i\partial_t) \equiv \sum_{m\geqslant 2} \beta_m (i\partial_t)^m/m!$ is the full dispersion operator, β_m is the mth order dispersion coefficient calculated at an arbitrary reference frequency ω_0, γ_K is the Kerr nonlinear coefficient of the gas, $R(t) = (1-\rho)\,\tilde{\delta}(t) + \rho\, h(t)$ is the normalized Kerr and Raman response function of the gas, $\tilde{\delta}(t)$ is the Dirac delta function, ρ is the relative strength of the noninstantaneous Raman nonlinearity, $h(t)$ is the causal Raman response function of the gas [16,20], the symbol $\otimes$ denotes the time convolution $[A \otimes B \equiv \int A(t-t')B(t')dt' = \int B(t-t')A(t')dt']$, c

is the speed of light, $k_0 = \omega_0/c$, ω_0 is the input pulse central frequency, $\omega_p = [e^2 n_e/(\epsilon_0 m_e)]^{1/2}$ is the plasma frequency associated to an electron density $n_e(t)$, e and m_e are the electron charge and mass, respectively, ϵ_0 is the vacuum permittivity, $\tilde{\alpha} = \tilde{\alpha}_1 + \tilde{\alpha}_2$ is the total loss coefficient, $\tilde{\alpha}_1$ is the fiber loss, $\tilde{\alpha}_2 = \frac{A_{\rm eff} U_I}{2|\Psi|^2}\,\partial_t n_e$ is the ionization-induced loss term [40], $A_{\rm eff}$ is the effective mode area, U_I is the ionization energy of the gas, $|\Psi|^2 = I A_{\rm eff}$, $|\Psi|^2_{\rm th} = I_{\rm th} A_{\rm eff}$, and n_T is the total number density of ionizable atoms in the fiber, associated to the maximum plasma frequency $\omega_T \equiv [e^2 n_T/(\epsilon_0 m_e)]^{1/2}$. The recombination process is safely neglected in these coupled equations since the pulse duration (of the order of tens of fs) is always shorter than the recombination time [32,41]. However, the recombination effects as well as the rearrangement of the electronic plasma due to ponderomotive forces should be included in the case of long-pulse propagation, making the problem considerably more difficult in the long-pulse regime [42,43].

Introducing the following rescalings and redefinitions, $\xi \equiv z/z_0$, $\tau \equiv t/t_0$, $\Psi_0 \equiv [\gamma_K z_0]^{-1/2}$, $\psi \equiv \Psi/\Psi_0$, $|\psi_{\rm th}| \equiv |\Psi|_{\rm th}/\Psi_0$, $r(\tau) \equiv R(t)\,t_0$, $\phi \equiv \frac{1}{2} k_0 z_0\,[\omega_p/\omega_0]^2$, $\phi_T \equiv \frac{1}{2} k_0 z_0\,[\omega_T/\omega_0]^2$, $\sigma \equiv \tilde{\sigma}\,t_0/[A_{\rm eff}\gamma_K\,z_0]$, and $\kappa \equiv U_I\,\tilde{\sigma}\,\epsilon_0\,m_e\,\omega_0^2/[k_0\,e^2]$, where $z_0 \equiv t_0^2/|\beta_2(\omega_0)|$ is the second-order dispersion length at the reference frequency ω_0 and t_0 is the input pulse duration [16]. The two coupled equations for floating pulses can be replaced by

$$[i\,\partial_\xi + \hat{D}(i\,\partial_\tau) + r(\tau) \otimes |\psi(\tau)|^2 - \phi + i\alpha]\psi = 0, \quad (5)$$

$$\partial_\tau \phi = \sigma(\phi_T - \phi)\big[|\psi|^2 - |\psi|^2_{\rm th}\big]\Theta\big(|\psi|^2 - |\psi|^2_{\rm th}\big), \quad (6)$$

where $\alpha = \kappa\,(\phi_T - \phi)\,[1 - |\psi|^2_{\rm th}/|\psi|^2]\,\Theta(|\psi|^2 - |\psi|^2_{\rm th})$, and the fiber losses are neglected.

III. PERTURBATION THEORY FOR SOLITONS

The effect of the Raman and ionization perturbations on the soliton dynamics can be studied by using the perturbation theory described in standard textbooks (e.g., Ref. [16]). Neglecting higher-order dispersion coefficients, i.e., $\beta_{m>2} = 0$, the solution of a perturbed nonlinear Schrödinger equation, $i\,\partial_\xi \psi + \frac{1}{2}\,\partial_\tau^2 \psi + |\psi|^2\psi = i\,\epsilon(\psi)$, is assumed to be $\psi(\xi,\tau) = A(\xi)\,\mathrm{sech}\{A(\xi)[\tau - \tau_p(\xi)]\}e^{-i\delta(\xi)\tau}$, where A is the soliton amplitude, τ_p is the temporal location of the soliton maximum, $\delta = (\omega - \omega_0)t_0$ is the normalized pulse frequency shift from the input central frequency, ω is the frequency, and $\epsilon(\psi)$ is the perturbation function. Substituting this *ansatz* in Eqs. (5) and (6), the following ordinary differential equations (ODEs) are obtained:

$$\frac{\partial \delta}{\partial \xi} = -\mathrm{Im}\left\{\int_{-\infty}^{+\infty} \epsilon(\psi)\tanh[A(\tau - \tau_p)]\,\psi^*\,d\tau\right\}, \quad (7)$$

$$\frac{\partial \tau_p}{d\xi} = -\delta + \frac{1}{A}\mathrm{Re}\left\{\int_{-\infty}^{+\infty} \epsilon(\psi)(\tau - \tau_p)\,\psi^*\,\partial\tau\right\}, \quad (8)$$

$$\frac{\partial A}{\partial \xi} = \mathrm{Re}\left\{\int_{-\infty}^{+\infty} \epsilon(\psi)\,\psi^*\,d\tau\right\}, \quad (9)$$

where Re and Im stand for real and imaginary parts.

In order to extract useful analytical information from Eqs. (5) and (6), we will start with the simplest case where we assume that the ionization loss and the threshold are negligible. Ignoring ionization loss is unrealistic unless the pulse under consideration has its maximum amplitude just above the threshold, in which case it does not feel strong plasma-induced decay. In this particular case, Eq. (6) can be solved analytically, $\phi(\tau) = \phi_T\{1 - \exp[-\sigma\int_{-\infty}^{\tau}|\psi(\tau')|^2 d\tau']\}$, with an initial condition $\phi(-\infty) = 0$, corresponding to the absence of any plasma before the pulse arrival. For a small ionization cross section, $\phi(\tau) \simeq \eta\int_{-\infty}^{\tau}|\psi(\tau')|^2 d\tau'$, where $\eta \equiv \sigma\phi_T$. Moreover, in the long-pulse limit one has $|\psi(\tau - \tau')|^2 \simeq |\psi(\tau)|^2 - \tau'\partial_\tau|\psi(\tau)|^2$ [16]. This allows the two coupled equations to be reduced to a single partial integrodifferential equation:

$$i\,\partial_\xi\psi + \hat{D}(i\,\partial_\tau)\psi + |\psi|^2\psi - \tau_R\psi\,\partial_\tau|\psi|^2 - \eta\psi\int_{-\infty}^{\tau}|\psi|^2 d\tau' = 0, \quad (10)$$

where $\tau_R \equiv \int_0^\infty \tau'\,r(\tau')\,d\tau'$. This equation shows clearly that the effect of ionization is essentially opposite to that of the Raman effect: the fourth term in Eq. (10) involves a *derivative* of the field intensity, while the fifth term involves an *integral* on the same quantity. Thus, one can conjecture that the ionization perturbation will lead to a soliton self-frequency blueshift, instead of a redshift. However, this is not an exact analogy because of thermodynamical reasons. In fact, the Raman effect acts on a soliton by constantly decreasing its central frequency, leaving its pulse shape in the time domain and in the frequency domain undeformed—in other words, the soliton continuously converts its coherent energy into incoherent optical phonons in the medium, and therefore the number of photons contained in the soliton does not change, and the overall entropy increases according to the second law of thermodynamics. However, in the photoionization-induced soliton blueshift described above, the soliton coherently receives energy from the medium (the plasma in this case). For this to be physically possible without breaking the second law of thermodynamics, the number of photons in the soliton must necessarily decrease—thus, the *unavoidable* plasma-induced losses cannot be eliminated on principle. The stronger the initial pulse intensity, the stronger the soliton blueshift, and the larger the plasma-induced losses, so that Eq. (10), which assumes small losses, would lose its validity. However, in the following we shall prove numerically that, when solitons decrease their amplitudes to just above the ionization threshold, their losses are very limited so that they can propagate for relatively long distances. This led us to naturally introduce the concept of *floating solitons*, i.e., those solitary pulses with maximum amplitude just a little above the threshold—the regime where ionization losses can be neglected and Eq. (10) maintains its validity [26].

Solving Eq. (10) with a perturbation function, $\epsilon(\psi) = -i\psi[\tau_R\partial_\tau|\psi|^2 + \eta\int_{-\infty}^{\tau}|\psi(\tau')|^2 d\tau']$, results in $A(\xi) = A(0) = A_0$, $\delta(\xi) = \delta_{\rm Raman}(\xi) + \delta_{\rm ion}(\xi) = -g\,\xi$, $\tau_p(\xi) = g\,\xi^2/2$, and $g = g_{\rm red} + g_{\rm blue}$, where $g_{\rm red} = +(8/15)\tau_R A_0^4$ and $g_{\rm blue} = -(2/3)\eta A_0^2$ [26]. Note that g can be positive, negative, or even zero, depending on the value of η, τ_R, and A_0. The precise rate for the self-frequency blueshift can be obtained using the exact formula of $\phi(\tau)$, $g'_{\rm blue} = \sigma^{-2}A_0^{-1}\phi_T[(1 - \sigma A_0) - (1 + \sigma A_0)\exp(-2\sigma A_0)]$, which

tends to $g_{\rm blue}$ for small values of σ, but starts to differ considerably from it for $A_0 > \sigma^{-1}$.

A further step can be applied to take into account the effect of the threshold intensity on the blueshift rate. For floating pulses, the ionization loss is not large and can be neglected to a good approximation. For such pulses, only a small portion of energy above the threshold intensity contributes to the electron-density buildup. In this case, $\phi(\tau) \simeq \eta \int_{-T}^{\tau' \leqslant T} [|\psi(\tau')|^2 - |\psi|_{\rm th}^2] d\tau'$, where $T = A_0^{-1} \mathrm{sech}^{-1}[|\psi|_{\rm th}/A_0]$. This formulation embeds the Heaviside function introduced in Eq. (6). Replacing the fifth term in Eq. (10) with the new definition of $\phi(\tau)$ and solving Eq. (7) results in

$$g_{\rm blue} = -\eta A_0^2 \left[\frac{2}{3} \tanh^3 \theta + \frac{|\psi|_{\rm th}^2}{A_0^2} (\theta \, \mathrm{sech}^2 \theta - \tanh \theta) \right], \tag{11}$$

with $\theta = A_0 T$. It can be seen that this expression tends to $-(2/3)\eta A_0^2$ for small $|\psi|_{\rm th}$.

The threshold intensity effect on the blueshift rate can also be alternatively estimated by writing Eq. (10) as

$$i \partial_\xi \psi + \hat{D}(i \partial_\tau) \psi + |\psi|^2 \psi - \tau_{\rm R} \psi \partial_\tau |\psi|^2 - \tilde{\eta} \psi \int_{-\infty}^{\tau} |\psi|^2 d\tau' = 0, \tag{12}$$

where $\tilde{\eta} = \eta \, \mu$ and

$$\mu = \frac{\int_{-T}^{T} \left[|\psi(\tau')|^2 - |\psi|_{\rm th}^2 \right] d\tau'}{\int_{-\infty}^{\infty} |\psi(\tau')|^2 d\tau'}. \tag{13}$$

The factor μ represents the ratio between the pulse energy contributing to plasma formation (from $-T$ to $+T$) and the total energy of the pulse; see Fig. 1(b). Thus, it takes into account the overestimation of the plasma density by neglecting the threshold intensity. As a consequence, one can simply prove that $g_{\rm blue} = -(2/3)\tilde{\eta} A_0^2$.

Moreover, the effect of the photoionization loss on the soliton amplitude and frequency shift can be studied numerically by solving the above ODEs with $\epsilon(\psi) = -i\psi[\eta \int_{-T}^{\tau' \leqslant T} (|\psi(\tau')|^2 - |\psi|_{\rm th}^2) d\tau' - i\alpha]$, where T is determined via its previous definition using the initial pulse amplitude, and the variation of the position T due to losses is neglected:

$$\begin{aligned} \frac{\partial A}{\partial \xi} &= -2\kappa \, \phi_{\rm T} \left(A \tanh \vartheta - |\psi|_{\rm th}^2 \, T \right), \\ \frac{\partial \delta}{\partial \xi} &= \eta \, A^2 \left[\frac{2}{3} \tanh^3 \vartheta + \frac{|\psi|_{\rm th}^2}{A^2} (\vartheta \, \mathrm{sech}^2 \vartheta - \tanh \vartheta) \right], \end{aligned} \tag{14}$$

$\vartheta = AT$. These equations can be solved numerically to determine the spatial dependence of the soliton amplitude and frequency shift, as shown in Fig. 2. Pulses with initially large intensities ($A_0^2 > |\psi|_{\rm th}^2$) have a boosted self-frequency blueshift. However, the ionization loss suppresses the soliton intensity after a short propagation distance to the floating-soliton regime, where the soliton can propagate for a long propagation distance with a limited blueshift and negligible loss. The maximum frequency shift is achieved when the soliton intensity goes below the photoionization threshold.

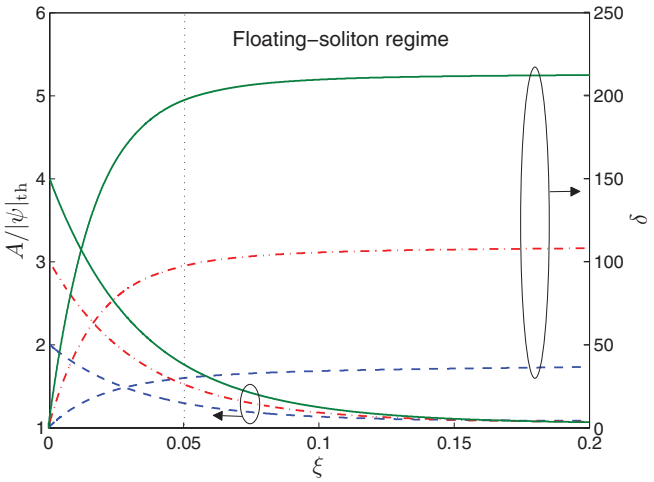

FIG. 2. (Color online) The spatial dependence of the soliton amplitude and frequency shift during a photoionization process for different initial pulse amplitudes.

IV. INVERTED GRAVITYLIKE BOUND STATES

The previous conclusions on the strong analogies between the photoionization shift and the Raman shift of solitons allow us to construct a kind of solitary wave that can be supported by both the Kerr and the ionization nonlinearities. This solitary waves will be analogous to the Raman bound solitons discovered experimentally in Ref. [44] and explained theoretically in Refs. [45–47]. In the noninertial reference frame of an accelerated soliton (with a new time coordinate $\zeta \equiv \tau - g\,\xi^2/2$), and by using the so-called Gagnon-Bélanger gauge transformation $\psi(\xi,\tau) = f(\zeta) \exp[i(q - g^2\,\xi^2/3 + g\,\tau)\,\xi]$ [48], Eq. (12) can be written as an integrodifferential equation:

$$\tfrac{1}{2} \partial_\zeta^2 f - U(\zeta) \, f = q \, f, \tag{15}$$

where ionization loss and higher-order dispersion are neglected; $U(\zeta) = g\,\zeta - |f|^2 + \tau_R \partial_\zeta |f|^2 + \tilde{\eta} \int_{-\infty}^{\zeta} |f|^2 d\zeta'$ is a potential, in which the first term is gravitylike; $q = A_0^2/2 - \tilde{\eta} A_0$ is the soliton wave number; and A_0 is the amplitude of the one-peak solitary solution of Eq. (15). In the case when only the Raman effect was present [9,10], a special kind of nonlinear metastable bound states has been found as a general solution for Eq. (15) [49–51]. Such bound states are multipeak stationary states (in the noninertial reference frame moving with acceleration $g_{\rm red}$), which are due to the Kerr effect complemented by the Raman nonlinearity [45–47]. Additional important features of this gravitylike potential analogy are presented in Ref. [52].

In the presence of a Raman-inactive gas (such as Argon) inside the HC-PCF, we have seen that the ionization process leads to a soliton acceleration in the time domain, and to a linear frequency shift toward the blue with a rate $g_{\rm blue}$. In this case, solitons will feel an inverted gravitylike linear potential, and the solution of Eq. (15) can be a multipeak stationary state with a negative slope opposite to the Raman case. An example of a two-peak bound state found numerically by using the shooting method is depicted in Fig. 3(a). Multipeak solitary solutions analogous to those found in Ref. [46] can also be

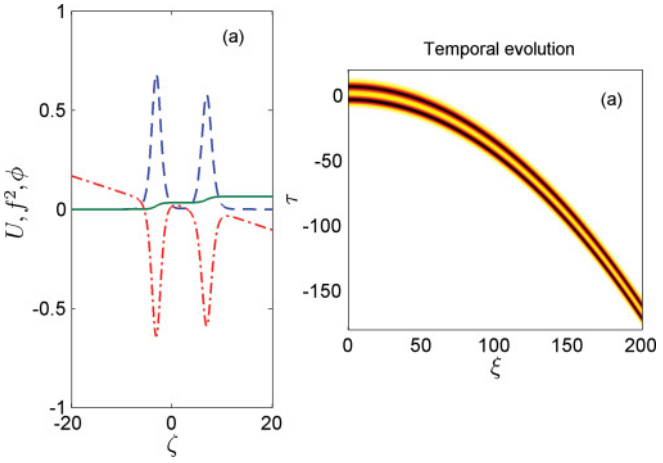

FIG. 3. (Color online) (a) A two-peak soliton stationary solution for a Raman-inactive gas with $\tilde{\eta} = 0.02$ and $q = 0.3$. The dashed-dotted red, dashed blue, and solid green curves represent the nonlinear potential U, the pulse intensity f^2, and the ionization field ϕ, respectively. (b) Temporal evolution of the two-peak soliton in a gas-filled HC-PCF fiber.

obtained. The propagation of the two-peak bound state found in Fig. 3(a) in a long HC-PCF is shown in Fig. 3(b).

The characteristics of a two-peak solitary solution—the temporal separation ζ_0 and the amplitude imbalance R between the two peaks—can be analytically determined. Consider a general two-peak solitary solution:

$$f(\zeta) = A_1 \mathrm{sech}[A_1(\zeta - \zeta_1)] + A_2 \mathrm{sech}[A_2(\zeta - \zeta_2)], \quad (16)$$

where $A_2 = R\,A_1$ and $\zeta_0 = \zeta_2 - \zeta_1$. In principle, a set of three algebraic equations is needed to determine A_1, ζ_0, and R. By substituting the above solution in Eq. (15), the first equation is obtained:

$$-g_{\mathrm{blue}}\zeta_0 = A_1^2(1 - R^2)/2 + \tilde{\eta}A_1(1 + R), \quad (17)$$

where $\tilde{\eta}$ is assumed to be the same for the two solitons. The last term on the right-hand side is due to the integration constant in the nonlinear potential $U(\zeta)$, and it is not present in the analogous expression for the pure Raman-bound states [i.e., $-g_{\mathrm{red}}\zeta_0 = A_1^2(1 - R^2)/2$] since the Raman effect is modeled in the equations by a derivative. By multiplying Eq. (15) by f^*, and integrating both sides, we obtain

$$\int_{-\infty}^{\infty} \left[\frac{1}{2} f^* \partial_\zeta^2 f - U(\zeta)\,|f|^2\right] d\zeta = q \int_{-\infty}^{\infty} |f|^2 d\zeta, \quad (18)$$

where the superscript $*$ denotes the complex conjugate. A second equation can be attained by substituting Eq. (16) into Eq. (18):

$$A_1^2(1 + R^3)/2 - \tilde{\eta}A_1(1 + 2R + R^2) - q(1 + R) \approx 0. \quad (19)$$

The set of three algebraic equations is completed by Eq. (15) evaluated at $\zeta = 0$. Thus, variables A_1, ζ_0, and R can be determined for a certain value of q.

Finally in Raman-active gases, solitons may feel either a gravitylike or an inverted gravitylike potential based on the sign of the total gravity acceleration $g = g_{\mathrm{red}} + g_{\mathrm{blue}}$. This means that the two-peak solitary solution can have either a positive or negative slope as depicted in panels (a) and (b), respectively, of Fig. 4. Two-peak solitons with a positive (negative) slope are obtained when the Raman (photoionization) process is dominant.

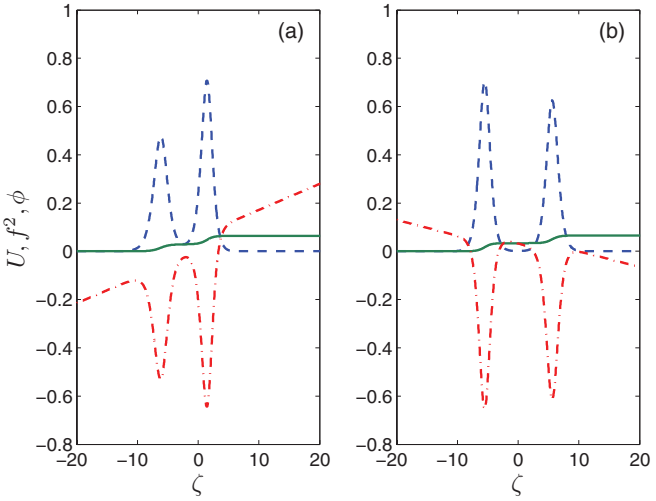

FIG. 4. (Color online) A two-peak soliton stationary solution in a Raman-active gas with $\tilde{\eta} = 0.02$ and $q = 0.3$. (a) Gravitylike bound states with $\tau_R = 0.1$. (b) Inverted gravitylike bound states with $\tau_R = 0.01$. The dashed-dotted red, dashed blue, and solid green curves represent the nonlinear potential U, the pulse intensity f^2, and the ionization field ϕ, respectively.

V. SOLITON DYNAMICS IN PLASMA

In this section, we will elaborate the results expressed in Ref. [26] concerning soliton dynamics in an ionized gas. Equations (5) and (6) can be numerically solved by using the split-step Fourier method [16] in order to fully describe the propagation of pulses in the presence of plasma. In this section, higher-order dispersion coefficients are assumed to be negligible, i.e., $\beta_{m>2} = 0$. The temporal and spectral evolution of a higher-order sech-pulse, with an initial intensity less than the threshold value, are depicted in panels (a) and (b), respectively, of Fig. 5. Panel (c) shows the variation of the ionization fraction along the fiber. An optical pulse pumped in the deep anomalous-dispersion regime of the fiber undergoes self-compression. When the pulse intensity exceeds the threshold value, a certain amount of plasma is generated due to gas ionization, and a fundamental soliton is ejected from the input pulse. The soliton central frequency continues to shift toward the blue due to the energy received from the generated plasma. However, due to the concurrent ionization loss, the soliton intensity gradually decreases until it goes below the threshold, stopping the pulse blueshift. A second ionization event accompanied by a second-soliton emission can take place by further self-compression of the input pulse based on its initial intensity.

A clear representation for the pulse dynamics in plasma is shown in Fig. 6, where the temporal profile of the pulse intensity $|\psi|^2$ is plotted at selected positions inside the fiber. The simulation parameters are similar to Fig. 5. Initially, $|\psi(\tau)|^2$ is insufficient for plasma ionization. Due to soliton breathing, the pulse passes through a self-compression stage which strongly enhances its maximum intensity [53]. The

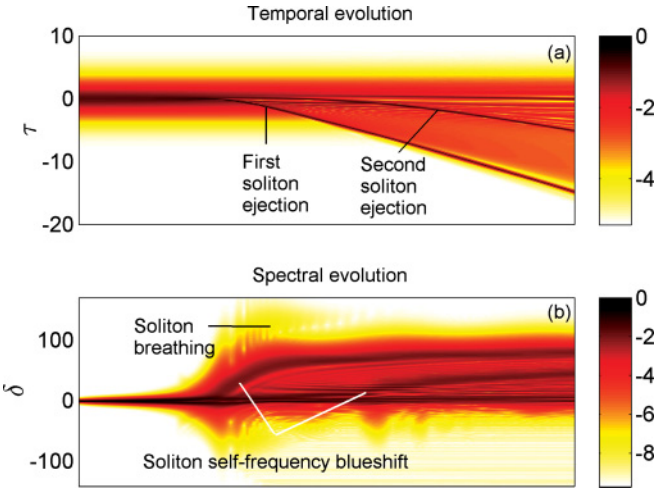

FIG. 5. (Color online) Temporal (a) and spectral (b) evolution of an energetic pulse propagating in an Ar-filled HC-PCF. The temporal profile of the input pulse is $N \operatorname{sech} \tau$, with $N = 8$, $t_0 = 50$ fs. All subsequent calculations in this paper assume the same pulse duration. The gas pressure is 5 bar. The panels show the ejection of two solitons that continue blueshifting until the ionization loss suppresses their intensities below the threshold value. Contour plots in this paper are given in a logarithmic scale. (c) Spatial dependence of the ionization fraction along the fiber.

amount of optical energy above the threshold intensity $|\psi|^2_{\text{th}}$ contributes to plasma formation that emits a blueshifted soliton. However, due to the ionization-induced loss, the soliton amplitude is attenuated to the regime where $|\psi(\tau)|^2 \gtrsim |\psi|^2_{\text{th}}$. Such pulses, the floating solitons, propagate for considerably long distances with minimal attenuation and limited blueshift. Based on the initial input pulse intensity, other solitons can also be emitted due to further self-compression. At the end, a train of floating solitons is generated. Indeed, Fig. 6 clearly

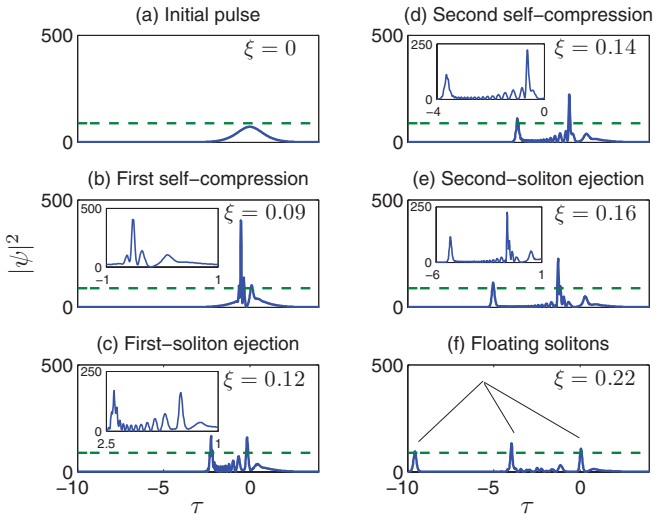

FIG. 6. (Color online) Intensity profile of a pulse in the time domain at different positions, ξ, inside an Ar-filled HC-PCF. The dashed red line represents the threshold intensity. The simulation parameters are similar to Fig. 5. Each panel is titled by its main feature. Insets are enclosed in panels for better view and more details.

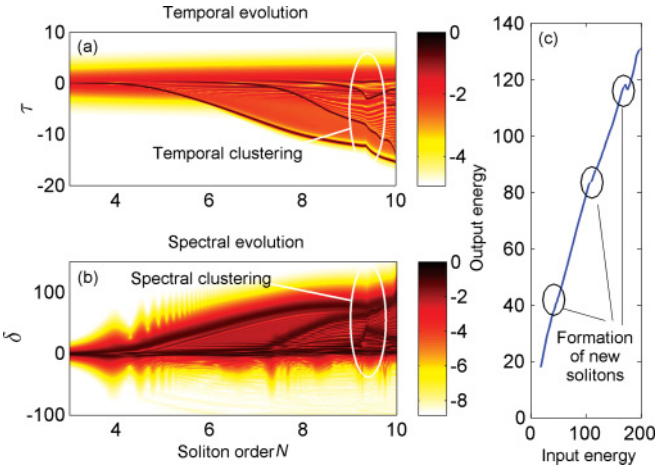

FIG. 7. (Color online) Dependence of the temporal (a) and spectral (b) outputs of an energetic pulse $N \operatorname{sech} \tau$ on the soliton order N. The fiber is an Ar-filled HC-PCF with length $\xi = 1/4$. The gas pressure is 5 bar. Temporal and spectral clustering occur at $N = 9.2$ due to the long-range nonlocal soliton interactions. (c) The output energy vs the input energy, to be compared with Fig. 2(d) of Ref. [23].

shows the formation of a series of floating solitons that exist and propagate for relatively long distances with their maximum amplitude just above the ionization threshold. These objects are completely unknown in conventional solid-core fiber optics. The fact that these results have been confirmed in concurrent experiments [23] is a very convincing proof of the validity of our master Eqs. (5) and (6).

We have also found an interesting nonlocal interaction between successive solitons due to the nonvanishing electron-density tail, when their temporal separation is shorter than the recombination time. Due to this interaction, a leading soliton can slow down the acceleration of a trailing soliton by an exponential factor. In the frequency domain, the leading soliton suppresses exponentially the blueshift of the trailing soliton. The reason is that the ionization field $\phi(\tau)$, created by the first soliton, decays at a relatively slow rate. This establishes a unique "nonlocal" interaction between this soliton and other temporally distant solitons.

These unprecedented dynamics are featured in Fig. 7, which shows the temporal and spectral dependence on the soliton order N assuming that the input pulse is $N \operatorname{sech} \tau$. A clustering between two or more distant solitons in both temporal and spectral domains is also observed at some "magic" input energy as a result of the interplay between the nonlocal interaction, ionization loss, and ionization threshold. The scenario is as follows: As long as the intensity of the first-emitted soliton, I_1, is above the threshold intensity I_{th}, it prevents the ejection of a second soliton due to the strong suppressive effect of the nonlocal interaction. As soon as I_1 approaches I_{th} by virtue of the ionization loss, the first soliton becomes a floating soliton. Thus, the blueshift and acceleration of this soliton are reduced significantly. Simultaneously, the second soliton can be emitted with its expected acceleration and blueshift due to the near disappearance of the nonlocal force induced by the first soliton. This allows the second soliton to catch up and cluster with the first soliton. In addition, the

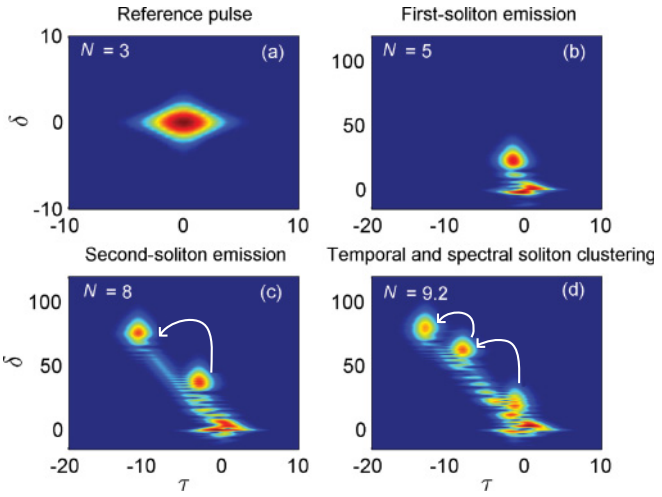

FIG. 8. (Color online) XFROG spectrograms for pulses with selected soliton order N in increasing order. The simulation parameters are similar to Fig. 7. (a) $N = 3, \xi = 0$. (b) $N = 5, \xi = 1/4$. (c) $N = 8, \xi = 1/4$. (d) $N = 9.2, \xi = 1/4$. Each panel is titled by its main feature. White arrows show the movement of the solitons.

spectra of the two solitons start to overlap and form spectral clustering. Similarly, when the intensity of the second soliton approaches I_{th} due to the ionization loss, a third soliton is ejected and allowed to cluster with the other two solitons. However, when the first two solitons are very close to each other, they push back the third soliton due to their *combined* nonlocal force. In fact, the dynamics after the clustering becomes too complicated to be interpreted in simple terms.

Figure 7(c) shows the output energy versus the input energy. The linear dependence of the output energy is slightly broken at the points which correspond to the ejection of new solitons. Our results show an excellent qualitative agreement with other nonanalytical numerical techniques [27] and with the experimental results of Ref. [23].

Cross-frequency-resolved optical gating (XFROG) spectrograms for pulses with initial temporal profile N sech τ and different initial intensities are depicted in the panels of Fig. 8, where (a) represents the reference pulse; (b) and (c) shows the emission of the first and second solitons, respectively; and (d) depicts the temporal and spectral clustering of the first two solitons and the emission of a third soliton.

VI. GENERATION OF DISPERSIVE WAVES

The contribution of the higher-order dispersion coefficients $\beta_{m>2}$ to the pulse dynamics starts to play a significant role as the central pulse wavelength moves toward the zero-dispersion wavelength (ZDW), where $\beta_2(\omega_0) \approx 0$. In fact, higher-order dispersion coefficients may lead to a phase-matching condition between two different waves—an optical pulse, with a central wavelength, which lies in the anomalous-dispersion regime and is close to the ZDW, and a dispersive resonance wave in the normal-dispersion regime [54,55]. Recently, this fact was implemented to achieve a coherent deep UV laser source by using an Ar-filled HC-PCF: Joly *et al.* [8] have obtained an 8% conversion efficiency from IR (320 nm) to UV (200 nm), where the output can be tuned easily via the pulse energy

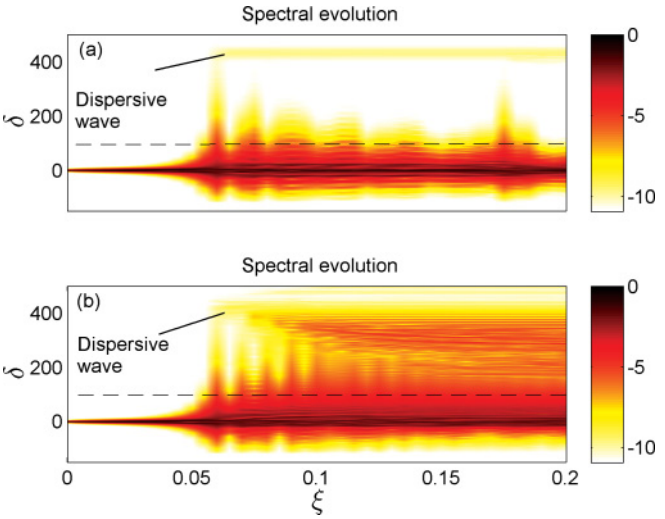

FIG. 9. (Color online) Spectral evolution of an energetic pulse N sech τ, with $N = 11$, under the influence of higher-order dispersion coefficients with (a) switching off the ionization process and (b) switching on the ionization process. The optical pulse central wavelength is 800 nm, and the gas pressure is 2 bar. The dotted line represents the ZDW.

and gas pressure. The pulse power level was kept below the ionization threshold to avoid any ionization-induced loss.

The aim of this section is to study the effect of photoionization on the dispersive-wave emission by the input pulse. The top (bottom) panel of Fig. 9 represents the spectral evolution of a higher-order sech pulse in a gas-filled HC-PCF, where the ionization is switched off (on). The pulse central wavelength is 800 nm, the ZDW is 432 nm ($\delta = 100$), and the resonant radiation frequency is located around 172 nm ($\delta = 430$). We find an enhancement in the dispersive-wave radiation via the photoionization process by more than an order of magnitude

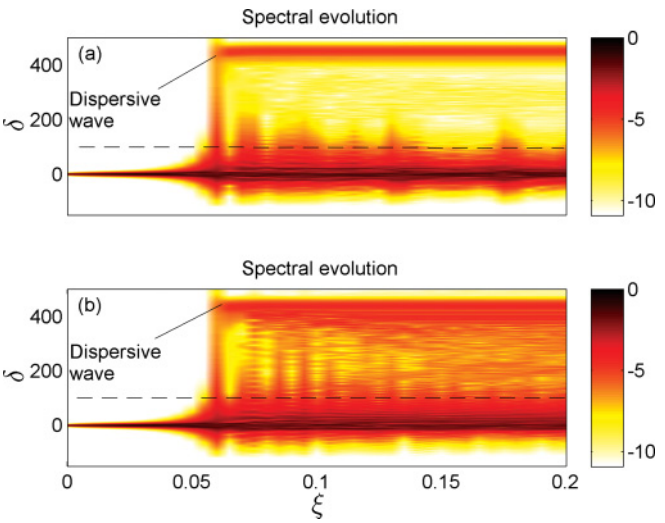

FIG. 10. (Color online) Spectral evolution of an energetic pulse under the influence of higher-order dispersion and shock terms with (a) switching off the ionization process and (b) switching on the ionization process. The simulation parameters are similar to Fig. 9 except that the shock operator τ_{shock} is included. The dotted line represents the ZDW.

TABLE I. Conversion efficiencies to the normal-dispersion regime for different gas pressures using an energetic pulse N sech τ. The other simulation parameters are similar to Fig. 10.

P[a] (bar)	ZDW[b] (nm)	DWW[c] (nm)	Υ_1[d] (%)	Υ_2[e] (%)
5	530	240	2.46	2.42
4	500	225	1.50	1.46
3	470	200	0.66	0.79
2	430	170	0.11	1.17

[a]Pressure.
[b]Zero dispersion wavelength.
[c]Dispersive wave wavelength.
[d]Conversion efficiency in the absence of ionization.
[e]Conversion efficiency in the presence of ionization.

due to the ionization-induced blueshift. Unlike the Raman process, where the pulse central wavelength is continuously redshifted away from the ZDW during propagation, the ionization-induced blueshift toward the ZDW enhances the spectral overlap between the dispersive waves and the input pulse tail, improving the conversion efficiency to the UV range.

The dispersion of Kerr nonlinearity is usually associated with effects such as self-steepening and optical shock formation [16]. Due to the absence of the Raman effect in kagomé-style HC-PCFs filled with noble gases, and due to the smallness of the group-velocity dispersion (GVD) in such fibers, the role of the Kerr nonlinearity dispersion has an unexpected importance. This effect can be studied by using Eqs. (3) and (4), where γ_K is replaced by $\gamma_K\,(1 + i\,\tau_{\rm shock}\,\partial_t)$ and $\tau_{\rm shock} = 1/\omega_0$ is the shock time [16]. The importance of the shock term is depicted in Fig. 10, where the simulation parameters are similar to Fig. 9 except that $\tau_{\rm shock}$ is included. Involving the shock term in the pulse dynamics increases the conversion efficiency to the normal-dispersion regime from 0.44% [Fig. 9(b)] to 1.1% [Fig. 10(b)] at the end of the fiber due to the spectral asymmetry of the pulse.

The conversion efficiencies from the pump pulse to the normal-dispersion regime for different gas pressures (using the same input pulse) in both the absence and presence of the photoionization process are provided in Table I. For a high gas pressure, the ZDW is too close to the pump central wavelength λ_0. This leads to a considerably high conversion efficiency due to a broad spectral overlap between the tail of the input pulse and the dispersive wave. On the other hand, the ionization-induced blueshift is relatively insignificant due to the negligible β_2 that does not allow an efficient pulse self-compression. We attribute the slight reduction in the conversion efficiency to the unavoidable ionization-induced loss. When the gas pressure is reduced, the ZDW moves away from λ_0. As a result, the dispersive wave would have been emitted in the deep UV ($<$ 200 nm) by the input pulse, with a small conversion efficiency. However, we find that the emission is strengthened by an order of magnitude due to the strong ionization-induced blueshift effect in this case.

VII. CONCLUSIONS

We have presented a detailed model based on the evolution of the complex pulse envelope to study pulse propagation in gas-filled HC-PCFs under the influence of the nonlinear photoionization-induced effects. By applying perturbation theory, we show that the photoionization process represents the exact counterpart of the Raman self-frequency redshift of solitons when their intensities are slightly above the threshold intensity. Expressions of the soliton self-frequency blueshift are derived in the presence and absence of the photoionization threshold. Moreover, the influence of the ionization loss on the soliton amplitude and the frequency shift is studied. By using the Gagnon-Bélanger gauge transformation, stationary negative-slope two-peak inverted gravitylike solitary solutions are obtained for pulses propagating in HC-PCFs filled by Raman-inactive gases. However, positive- or negative-slope two-peak solitary solutions can also be attained in the presence of a tunable Raman-active gas. The pulse dynamics, obtained by using the split-step Fourier method, shows the soliton emission, breakup, and blueshift. Furthermore, we find unconventional long-range nonlocal interactions between successive solitons due to the nonvanishing electron-density tail. The interplay between this unprecedented interaction, the ionization-induced loss, and the ionization threshold yields a spectral and temporal clustering between distant solitons. Finally, in the presence of higher-order dispersion coefficients and the shock operator, we find that plasma formation via photoionization can strengthen the dispersive-wave radiation in the deep UV ($<$200 nm), assisted by the absence of the Raman effect in noble gases.

ACKNOWLEDGMENTS

We would like to thank John C. Travers, Philip Hölzer, Wonkeun Chang, Nicolas Y. Joly, and Philip St. J. Russell for useful discussions. This research is funded by the German Max Planck Society for the Advancement of Science.

[1] P. St. J. Russell, Science **299**, 358 (2003).
[2] P. St. J. Russell, J. Lightwave Technol. **24**, 4729 (2006).
[3] J. C. Travers, W. Chang, J. Nold, N. Y. Joly, and P. St. J. Russell, J. Opt. Soc. Am. B **28**, A11 (2011).
[4] F. Benabid, J. C. Knight, G. Antonopoulos, and P. St. J. Russell, Science **298**, 399 (2002).
[5] A. Abdolvand, A. Nazarkin, A. V. Chugreev, C. F. Kaminski, and P. St. J. Russell, Phys. Rev. Lett. **103**, 183902 (2009).
[6] A. Nazarkin, A. Abdolvand, A. V. Chugreev, and P. St. J. Russell, Phys. Rev. Lett. **105**, 173902 (2010).
[7] O. H. Heckl *et al.*, Appl. Phys. B **97**, 369 (2009).
[8] N. Y. Joly, J. Nold, W. Chang, P. Hölzer, A. Nazarkin, G. K. L. Wong, F. Biancalana, and P. St. J. Russell, Phys. Rev. Lett. **106**, 203901 (2011).
[9] E. M. Dianov, A. Ya. Karasik, P. V. Mamyshev, A. M. Prokhorov, V. N. Serkin, M. F. Stel'makh, and A. A. Fomichev, JETP Lett. **41**, 294 (1985).
[10] F. M. Mitschke and L. F. Mollenauer, Opt. Lett. **11**, 659 (1986).
[11] J. P. Gordon, Opt. Lett. **11**, 662 (1986).

[12] K. J. Blow and D. Wood, IEEE. J. Quantum Electron. **25**, 2665 (1989).

[13] V. N. Serkin, T. L. Belyaeva, G. H. Corro, and M. A. Granados, Quantum Electron. **33**, 325 (2003).

[14] V. N. Serkin, T. L. Belyaeva, G. H. Corro, and M. A. Granados, Quantum Electron. **33**, 456 (2003).

[15] L. F. Mollenauer and J. P. Gordon, *Solitons in Optical Fibers: Fundamentals and Applications* (Elsevier, New York, 2006).

[16] G. P. Agrawal, *Nonlinear Fiber Optics*, 4th ed. (Academic, San Diego, 2007).

[17] J. M. Dudley and J. R. Taylor, *Optical Fiber Supercontinuum Generation* (Cambridge University Press, Cambridge, 2010).

[18] V. N. Serkin and V. A. Vysloukh, in *Nonlinear Guided Wave Phenomena*, Technical Digest, TUB 14 (Optical Society of America, Washington, DC, 1993), pp. 236–239.

[19] S. P. Stark, A. Podlipensky, and P. St. J. Russell, Phys. Rev. Lett. **106**, 083903 (2011).

[20] E. E. Serebryannikov and A. M. Zheltikov, Phys. Rev. A **76**, 013820 (2007).

[21] A. B. Fedotov, E. E. Serebryannikov, and A. M. Zheltikov, Phys. Rev. A **76**, 053811 (2007).

[22] P. Hölzer, W. Chang, J. Nold, J. C. Travers, A. Nazarkin, N. Y. Joly, and P. St. J. Russell, in *CLEO:2011 - Laser Applications to Photonic Applications, OSA Technical Digest (CD)* (Optical Society of America, 2011), p. CMJ3.

[23] P. Hölzer, W. Chang, J. C. Travers, A. Nazarkin, J. Nold, N. Y. Joly, M. F. Saleh, F. Biancalana, and P. St. J. Russell, Phys. Rev. Lett. **107**, 203901 (2011).

[24] J. Nold, P. Hölzer, N. Y. Joly, G. K. L. Wong, A. Nazarkin, A. Podlipensky, M. Scharrer, and P. St. J. Russell, Opt. Lett. **35**, 2922 (2010).

[25] M. Geissler, G. Tempea, A. Scrinzi, M. Schnürer, F. Krausz, and T. Brabec, Phys. Rev. Lett. **83**, 2930 (1999).

[26] M. F. Saleh, W. Chang, P. Hölzer, A. Nazarkin, J. C. Travers, N. Y. Joly, P. St. J. Russell, and F. Biancalana, Phys. Rev. Lett. **107**, 203902 (2011).

[27] W. Chang, A. Nazarkin, J. C. Travers, J. Nold, P. Hölzer, N. Y. Joly, and P. St. J. Russell, Opt. Express **19**, 21018 (2011).

[28] P. Kinsler, Phys. Rev. A **81**, 013819 (2010).

[29] A. M. Kosevich, Physica D **41**, 253 (1990).

[30] D. J. Mitchell, A. W. Snyder, and L. Poladian, Phys. Rev. Lett. **77**, 271 (1996).

[31] M. Wegener, *Extreme Nonlinear Optics* (Springer-Verlag, Berlin, 2005).

[32] P. Sprangle, J. R. Peñano, and B. Hafizi, Phys. Rev. E **66**, 046418 (2002).

[33] G. L. Yudin and M. Y. Ivanov, Phys. Rev. A **64**, 013409 (2001).

[34] V. S. Popov, Phys.-Usp. **47**, 855 (2004).

[35] G. Gibson, T. S. Luk, and C. K. Rhodes, Phys. Rev. A **41**, 5049 (1990).

[36] S. Augst, D. D. Meyerhofer, D. Strickland, and S. L. Chint, J. Opt. Soc. Am. B **8**, 858 (1991).

[37] L. V. Keldysh, Sov. Phys. JETP **20**, 1307 (1965).

[38] M. V. Ammosov, N. B. Delone, and V. P. Krainov, Sov. Phys. JETP **64**, 1191 (1986).

[39] E. Esarey, P. Sprangle, J. Krall, and A. Ting, IEEE J. Quantum Electron. **33**, 1879 (1997).

[40] E. E. Serebryannikov, E. Goulielmakis, and A. M. Zheltikov, New J. Phys. **10**, 093001 (2008).

[41] W. M. Wood, C. W. Siders, and M. C. Downer, IEEE Trans. Plasma Sci. **21**, 20 (1993).

[42] P. M. Bellan, *Fundamentals of Plasma Physics* (Cambridge University Press, Cambridge, 2006).

[43] R. O. Dendy, *Plasma Dynamics* (Oxford University Press, New York, 1990).

[44] A. Podlipensky, P. Szarniak, N. Y. Joly, C. G. Poulton, and P. St. J. Russell, Opt. Express **15**, 1653 (2007).

[45] A. Hause, T. X. Tran, F. Biancalana, A. Podlipensky, P. St. J. Russell, and F. Mitschke, Opt. Lett **35**, 2167 (2010).

[46] T. X. Tran, A. Podlipensky, P. St. J. Russell, and F. Biancalana, J. Opt. Soc. Am. B **27**, 1785 (2010).

[47] A. Hause and F. Mitschke, Phys. Rev. A **82**, 043838 (2010).

[48] L. Gagnon and P. A. Bélanger, Opt. Lett. **15**, 466 (1990).

[49] N. Akhmediev, W. Królikovski, and A. J. Lowery, Opt. Commun. **131**, 260 (1996).

[50] A. V. Gorbach and D. V. Skryabin, Phys. Rev. A **76**, 053803 (2007).

[51] A. V. Gorbach and D. V. Skryabin, Nature Photonics **1**, 653 (2007).

[52] V. N. Serkin, A. Hasegawa, and T. L. Belyaeva, Phys. Rev. Lett. **98**, 074102 (2007).

[53] T. X. Tran and F. Biancalana, Phys. Rev. A **79**, 065802 (2009).

[54] A. V. Husakou and J. Herrmann, Phys. Rev. Lett. **87**, 203901 (2001).

[55] I. Cristiani, R. Tediosi, L. Tartara, and V. Degiorgio, Opt. Express **12**, 124 (2004).